Dice-and-fill single element octagon transducers for next generation 3D USCT

Michael Zapf[1], Patrick Pfistner[1], Claudio Imbracio Liberman[1], Koen van Dongen[2], Nico de Jong[2], Benjamin Leyrer[1], Hartmut Gemmeke[1], Nicole V. Ruiter[1]

[1]*Karlsruhe Institute of Technology, Eggenstein-Leopoldshafen, Germany*
E-Mail: michael.zapf@kit.edu
[2]*Delft University of Technology, Delft, Netherlands*

Abstract

At the Karlsruhe Institue of Technology (KIT), a 3D-Ultrasound Computer Tomography (3D-USCT) medical imaging system for early breast cancer detection is currently developed. With the next generation of 3D-USCT 2.5, the current region of interest (ROI) of 10 x 10 x 10 cm³ shall be increased to 20 x 20 x 20 cm³ to allow reliable imaging results also for bigger female breasts. Therefore, the opening angle (OA) of the future transducers should be increased to approx. 60 ° at 3 dB while other characteristics such as bandwidth (BW) and resonance frequency should be preserved or even improved. Based on the current dice-and-fill approach in transducer production, optimization is performed on piezoelectric sensor geometry and size, type and structure of matching and backing layer and interconnection technology of the several parts of the transducer.

Keywords: US transducer, composite materials, SAFT imaging, dice-and-fill

1 Introduction

Breast cancer is the most common cancer in females in the world [1, 2].The spreading probability of the tumor and thus the chances of survival are correlated to its size [3]. Therefore, early detection plays a vital role in reducing the mortality of breast cancer.

KIT developed a 3D USCT imaging system for early breast cancer detection [4] [5] [6]. Imaging is achieved by Synthetic Aperture Focusing Technique (SAFT) using a multistatic setup of 2041 ultrasound transducers, grouped in 157 Transducer Array Systems (TAS) embedded in a semi-elliposoidal aperture (Figure 1). A center frequency of 2.5 MHz is

applied. The bandwidth (BW) and opening angle (OA) at 3 dB amount to 1 MHz and 36 °, respectively. The fundamental connection between an ultrasound transducer's emission and reception sensitivity in the azimuth and elevation angle space is the tranducer's aperture size.

Finite element (FE) simulations have shown that a reduction in size of the current generation transducer elements by roughly a factor 2 from 900 µm to 500 µm is required to realize an OA of 60 ° at 3 dB. Wave simulations also revealed that a circular instead of the current rectangular aperture will result in additional homogeneity of the sound field.

As circular sensors are difficult to produce in the dice-and-fill approach, octagon shaped transducers are built for USCT 2.5. The octagon shape can be achieved with the established dice-and-fill technique by adding 2 sawing cuts. Furthermore, inspired by compressive sensing, an irregular distribution of the sensor elements on the TAS is applied which covers almost the full surface area of US transducer. Further improvements are introduced regarding connectivity and bandwidth.

2 Motivation

2.1 3D USCT 2.0 current status

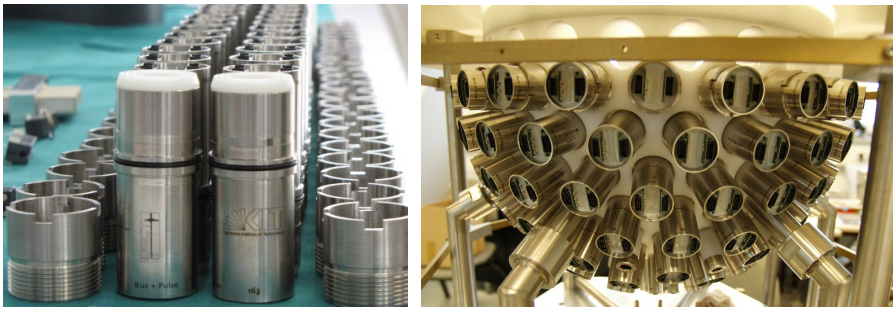

Figure 1: Left: USCT 2.0 TAS systems transducers before assembly in the final system. Right: Semi-ellipsoidal aperture of USCT 2.0

The current USCT 2.0 system covers a ROI of 10 x 10 x 10 cm^3. Results from the clinical trial with the University hospital Jena indicated that a bigger ROI is beneficial to cover a broader range of breasts and adapt also to the buoyance broadening effect of floating breasts [5]. Each of the 157 TAS consists of 13 rectangular transducer elements 0.9 x 0.9 mm in size [7]. One TAS consists of four emitters, nine receivers which are regularly distributed in a square grid, covering just the inner part of the TAS (Figure 2).

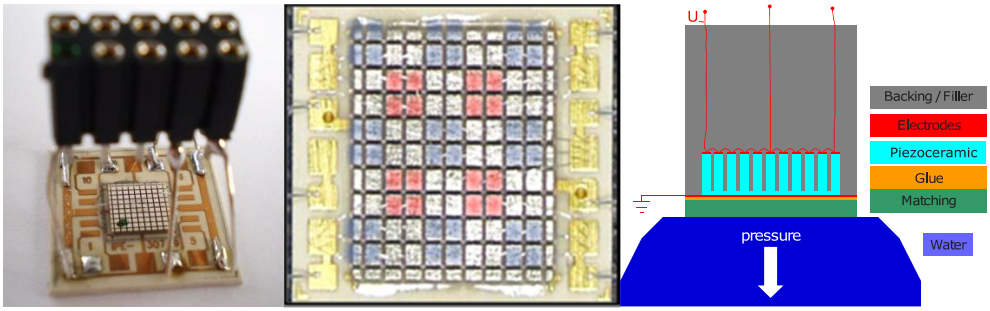

Figure 2: Left: Inner part of one TAS of USCT 2.0. Middle: Closer view on the piezoelectric elements. Four squares are connected to form one receiver (blue) or emitter (red). Right: Schematic side-view on one TAS of USCT 2.0.

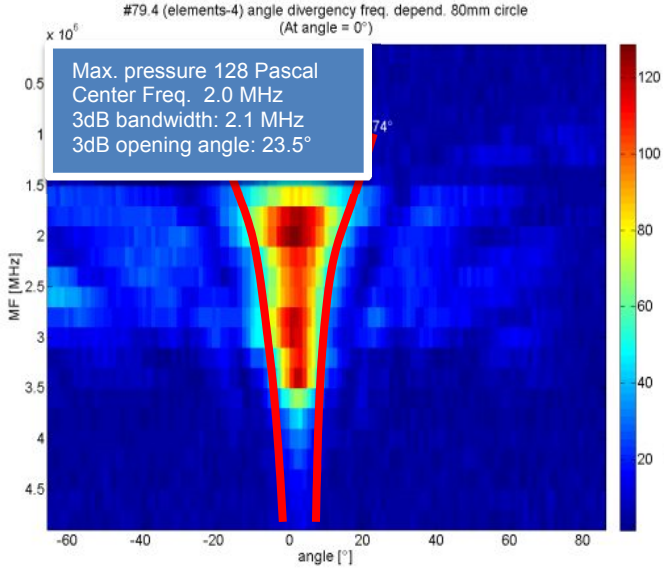

Figure 3: Frequency over angle for one element of one TAS of USCT 2.0. Given with red-lines approx. the frequency dependend 3dB opening angle.

2.2 Design considerations for next generation 3D USCT

For next generation 3D USCT (called 3D USCT 2.5) several should be improved contribute to a homogenous illumination and imaging contrast.

2.2.1 Opening angle (OA)

The benefit of an increased OA is schematically shown in Figure 4.

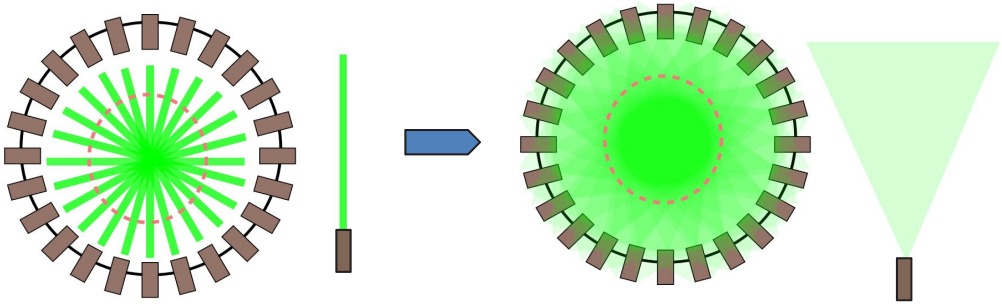

Figure 4: Illumination of an exemplary 3D-USCT system (top down view) for transducers with a small OA (left) compared to transducers with a larger OA (right).

2.2.2 Bandwidth

The BW of the transducers should be increased, as a larger BW better contrast in SAFT images, see Fig. 6. An increased coverage of the K-space, the spatial Fourier domain, can be achieved by broadening the bandwidth of the transducers. [8] Also, full wave inversion schemes and transmission tomography benefits from lower frequency components included in a broader bandwidth which covers also lower frequency down to 0.5 MHz.

2.2.3 Irregular distribution of sensor

An irregular distribution of the elements leads to greater coverage of the ROI and more homogeneous illumination. This is inspired by the "compressive sampling" concept now utilized in many apertures of various imaging systems as also ultra sound imaging systems.

2.2.4 Reduction in sparsity of sampling

An upgrade from 13 to 17 elements is performed. There are still nine receivers but the number of emitters has been doubled from four to eight emitters. Electronic constraints inhibit an upgrade to 9 emitters for symmetric emitter/receiver distribution. More emitters reduce the sparsity in imaging, leading to a more homogeneous coverage of the ROI. The final transducer distribution is shown in Figure 14.

2.3 Simulations

2.3.1 MATLAB

Ultrasound wavefield emission simulations for different surface geometries ("transducer apertures") have been performed as "piston model". As it is well known from antenna and

transducer design, there is an reciprocal relationship between the element / aperture size, and the directivity / opening angle of the sound beam. A reduction in transducer sidelength /diameter from 900 µm to 550 µm should lead to an increase in OA to 50 °-60 ° at 3 dB.

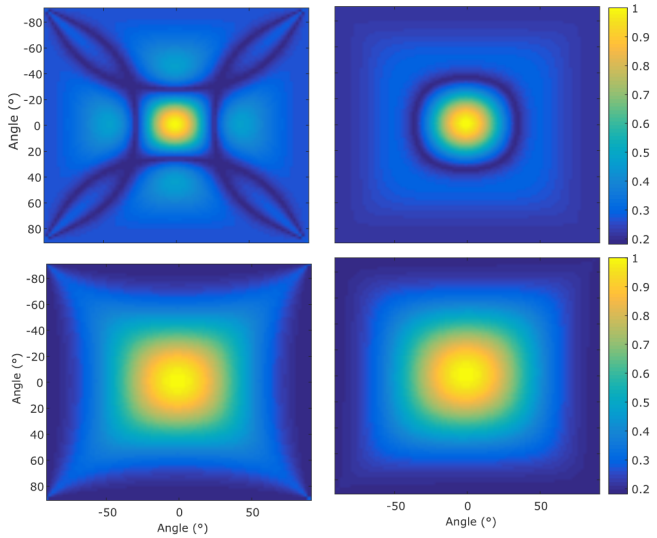

Figure 5: MATLAB aperture piston model simulations: US sound field for rectangular 0.9 mm (upper left), rectangular 0.4 mm (lower left), circular 0.94 mm (upper right) and circular 0.45 mm (lower right).

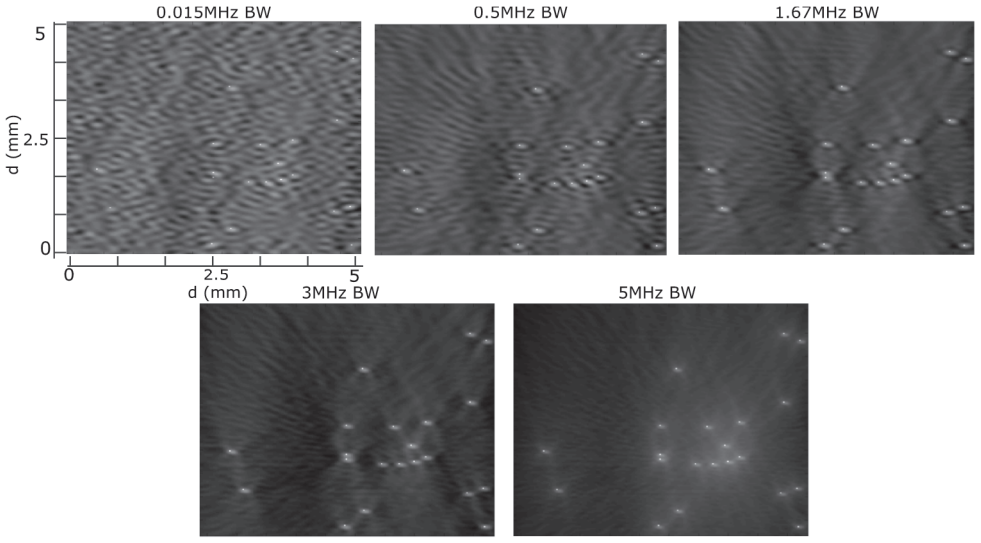

Figure 6: SAFT simulations for many point scatterers for varying BW. Contrast increases for broader bandwidth, while the resolution is more or less retained.

Circular elements express a more homogeneous sound over field compared to rectangular elements. (Figure 5).

SAFT simulations have been performed on point scatterers with varying BW (Figure 6). The results show that for SAFT image reconstruction, more BW leads to higher contrast in the images.

2.3.2 KLM

KLM simulations have been performed to find the ideal matching layer thickness for a broad BW. Simulations on TMM4 as a matching layer are shown in Figure 7. In the given configuration the resonance was the broadest for a 200 µm TMM4 layer due to two resonance peaks.

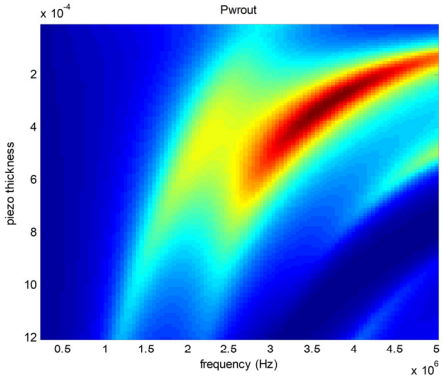

Figure 7: KLM model showing piezo thickness over frequency for a 200µm TMM4 matching layer with varying PZT thickness on the Y axis. X axis give the frequency range.

2.3.3 Finite element simulation

As 1D KLM simulations are insufficient to analyze lateral and shear wave effects of a design, a higher spatial dimensional simulation was utilized. Finite element (FE) simulations in 3D and 2D were performed. Also the impact of various materials on the Transducer performance were analyzed. PZflex was used as standard tool for piezoactive materials and non-piezoactive materials. The spatial properties of the transducer design was meshed with at least 3 times spatial sampling. Temporla sampling was derived automatically by the simulation tool, exported was the sound pressure field in each element in the water in the farfield in 2 to 6 cm distance.

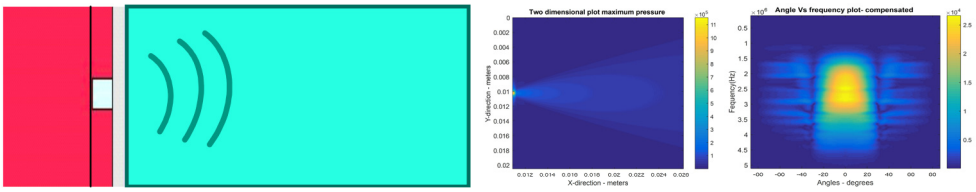

Figure 8: Left: Exemplary 2D PZFlex simulation model spanning 6cm in x and 2 cm in Y: Red: Backing + filling PU + Tungsten (12 MRayl): Red + bright blue: Piezofibrecompositedisc. (CeramTec Sonox 505 14.2 MRayl). Grey: Matching (TMM4 ca. 6.3 MRayl). Blue: Water (1.5 MRayl). Middle: Left: two-dimensional pressure plot X over Y, simulated by PZFlex for the setup described. Right: frequency over angle plot for the same setup.

3 Approach and method

First, the final transducer design approach will be presented. Afterwards, the individual process steps in the complex transducer production and their accompanying challenges and ideas are explained in more detail.

3.1 Transducer design and built up process

The Transducer Array System is built up starting from the backing where a 5 mm thick PVC substrate (Figure 13) with 2mm conical holes at the locations of the sensor elements acts as a base substrate on which top-side a flex-print is glued (Figure 10 right), providing the connectivity for the individual transducer elements. Pin holes guarantee alignment of the flex print and backing PVC.

A PU-tungsten composite material is molded into the holes (Figure 21 left), degassed and cured at room temperature over night.

Small PZT slabs of 700µm x 700µm are glued on copper pads of the flexprint with low temperature curing silver glue. Next, the square elements are shaped into octagons with a width of 550µm with a wafer dicing saw (Figure 16).

On the waterside, a matching layer is glued onto the piezoelectric sensor also with conductive silver-glue providing the common ground connection. Defined distance and parallelism is provided by a precise laser-cut spacer ring (Figure 18).

Two pins fix the rear part of the flex-print. A multi-channel plug ensures easy electrical connection to the back-end electronics (Figure 21 middle). The complete structure is waterproofed and mechanically stabilized with a hard-rubber like PU (Figure 19 left). A schematic side-view of the whole setup is shown in figure 9.

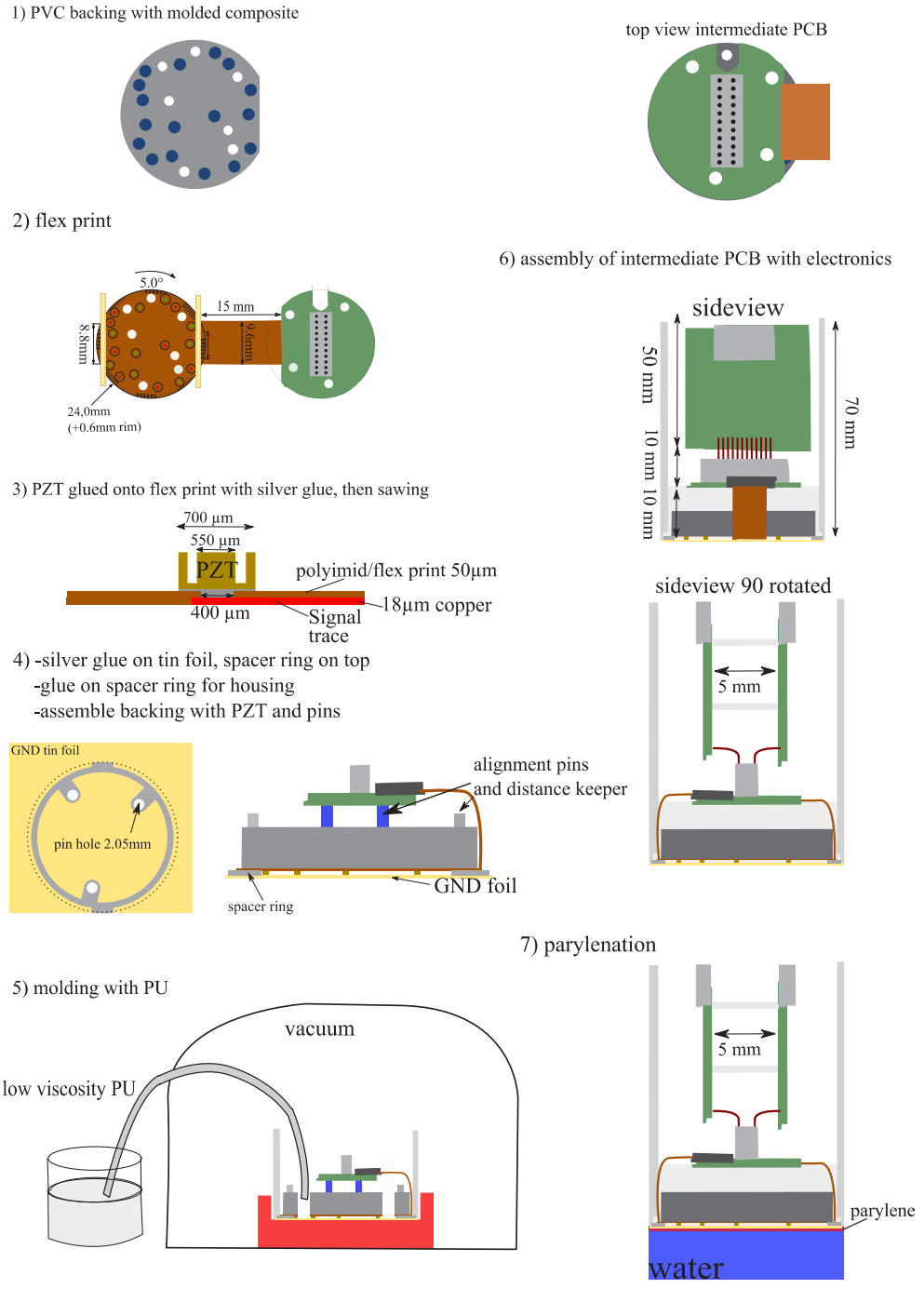

Figure 9: schematic of the whole build-up process for one TAS of next generation.

Electrical characterization was performed with a phase-impedance analyzer for all piezoelectric elements. Ultrasound characteristics were evaluated quantitatively with a hydrophone in a 3-axis water tank for selected sample transducers [8, 9].

3.2 PCB design

A Flexprint design was choosen as PCB base for electrical connectivity for the transducers.

Molding tests with the backing composite material led to bulging of the flex print. In response, four pin holes to span the foil have been added to facilitate molding. The layout and final product are shown in Figure 10.

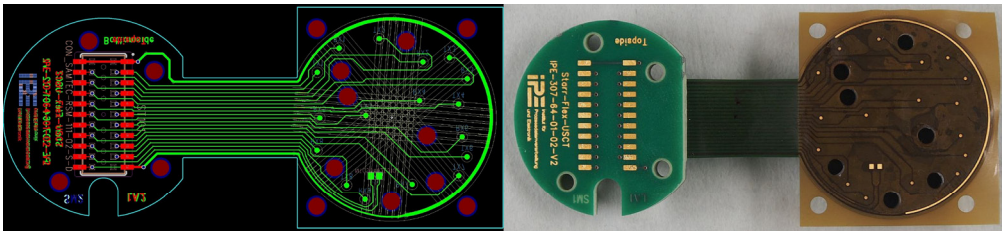

Figure 10: Flexprint PCB layout (left) and flex-print prototype v2 glued on a PVC substrate (right).

3.3 Composite materials

Research was conducted in the field of composite material to find possible matching and backing layers. The focus has been set on backing materials. A strongly attenuating composite of PU and tungsten powder was developed [10]. Acoustic impedance values of up to 11 MRayl are realizable. The improved acoustic matching to the rear improves the BW of the transducer by coupling US energy into the backing and attenuating the sound wave before reentering the piezo element. Degassing of the compound is difficult but possible with addition of a defoamer. Figure 11: 10 cm long rod of developed PU-tungsten composite material (left) and its lower part under the microscope (right). Degassing is possible, no major air inclusions are visible.

3.4 Backing

3.4.1 V1: Completely molded backing

First, tests were performed to investigate the molding ability of the backing composite with integrated pins of 2 mm in diameter. Tests have been successful (Figure 12). Next, a metal form with the actual TAS dimension has been built with alignment pin holes. The molded backing turned out to be not planar enough for the requirement of 20µm tolerancy.

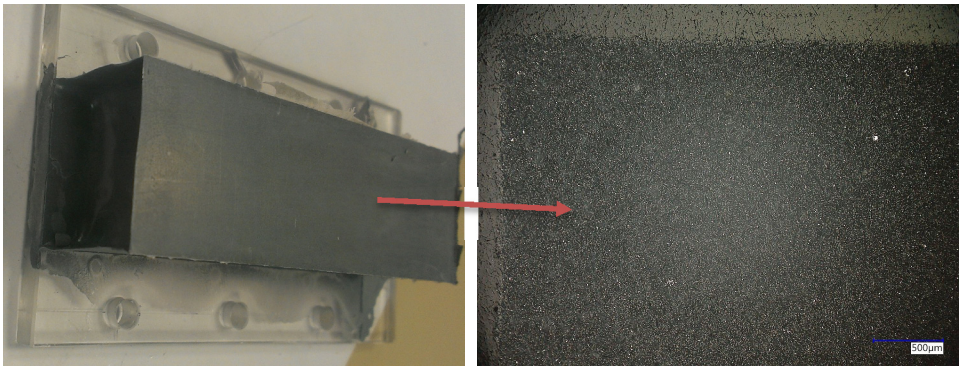

Figure 11: 10 cm long rod of developed PU-tungsten composite material (left) and its lower part under the microscope (right). Degassing is effective; no major air inclusions are visible.

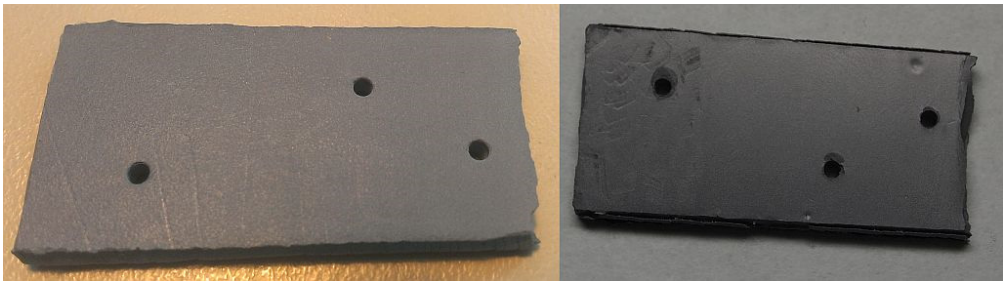

Figure 12: PU-tungsten composite integration test. The material shows surface roughness of the Teflon mold.

3.4.2 PVC substrate with molding of holes

As a completely molded backing proved to be difficult to realize, a combination of a planar backing substrate and molding was proposed. A PVC substrate with 2 mm holes behind the piezo locations was manufactured. The inner walls of the bore holes were parallel. Degassing of the backing composite through the holes was not possible properly.

An improved version with conical holes to the rear side to facilitate degassing (Figure 13) was later done. The end of the bore hole are rounded on the flex print side to facilitate plan parallel gluing of the flex print onto the PVC substrate.

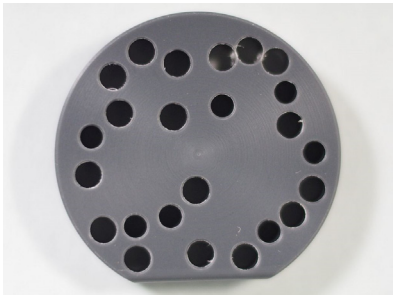

Figure 13: PVC substrate for the rear side for TAS 2.5 with high planarity and conical bore holes.

3.5 Positioning of piezos

3.5.1 V1

To increase the accuracy tolerance in x and y, larger PZT slabs of 1.5 mm side length are positioned onto the target locations with the pick and placer machine. Hereby, the x,y alignment accuracy is increased to ± 500 µm. In this configuration, the piezo has to be cut through completely. As the flex foil is 50 µm in thickness, the tolerance in z is reduced to ± 10 µm to not cut the leads.

3.5.2 V2

In order to increase the z tolerance at the expense of x, y tolerance, the piezos are decreased in side length to 700 µm. This reduces the x, y tolerance to ± 100 µm. Now, the residual piezo parts after sawing are so small that they mostly break during sawing.

In case the residual parts don't break, they are small enough that no complete cut-through is needed. Simulations have shown that sub-structuring to half or three quarter depth does not have a significant influence on acoustic performance of the transducer [11].

3.6 Sawing

The wafer dicing saw needs fiducial marks on opposite sides of the flex print every 45 ° for correct alignment of the sample. They are achieved by generating a regular octagon grid over the whole size of the TAS (Figure 14) and deleting the lines, but leaving the last few millimeters on the edge of the circular aperture. First tests with a fully automatized sawing procedure led to significant deviations from the desired octagon grid.

Therefore, the program has been split into two subprograms for 0 °/90 ° and 45 °/135 °. Before running each of these programs, a manual optical alignment on the fiducial marks or on the sawing traces is performed. These steps comprise possible errors.

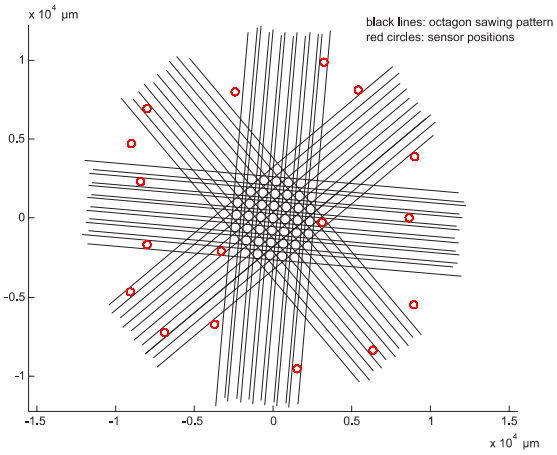

Figure 14: Transducer distribution for USCT TAS 2.5 (red circles). Black lines show the octagon sawing pattern that constrains the available sensor positions to its regular grid.

For a series production of the transducers, a fully automatized sawing process without manual interruption is aimed for. First measurements on the octagon shaped transducers expressed a significantly smaller opening angle than expected by the PZFlex simulations. Lateral waves are suggested to virtually increase the aperture, thereby decreasing the OA.

To reduce the influence of lateral waves, sub-structuring of the octagons into four parts (see Figure 16: Left: Test of additionally sub-structuring octagon. Right: TAS 2.5 prototype assembled with single element octagon dice-and-fill transducers.) is a possible solution. The decreased lateral dimensions of the sensor shift lateral modes to higher frequencies where they do not interfere with the USCT center frequency.

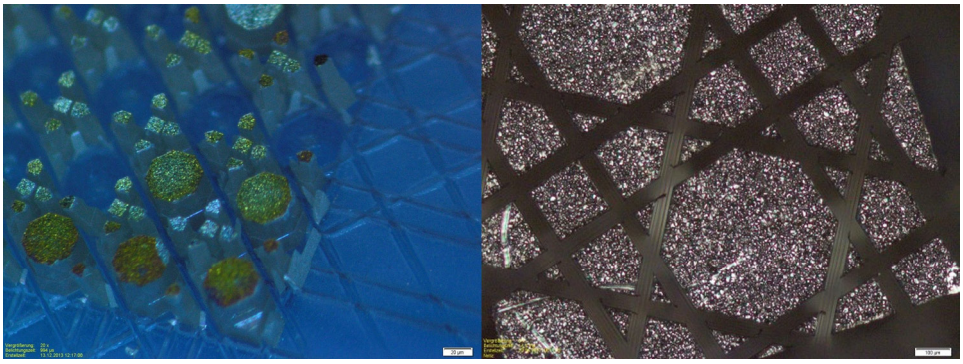

Figure 15: Octagon-shaped sensors after sawing, photos from a microscope.

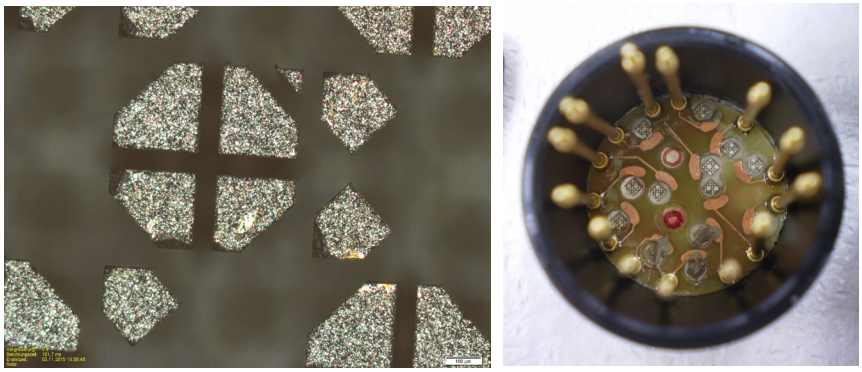

Figure 16: Left: Test of additionally sub-structuring octagon. Right: TAS 2.5 prototype assembled with single element octagon dice-and-fill transducers.

3.7 Gluing

In the first build ups a significant portio, 20-30 % of the sensors fell of during the sawing process. Further tests indicated improper heat curing of the silver glue. An optimized hardware setup improved the temperature profile while curing for one hour. Another improvement of the conductive silver glue utilization was an automated centrifugal mixer which ensured better homogeneity and viscosity. Additionally, quantitative analysis of the mechanical strength of the piezo/flex-print connection is needed to understand the reason for the failures of the piezo elements, to optimize the amount of glue printed, the curing profile and possibly also the type of glue.

In a first test series, PC3000 silver glue was stencil-printed on Cu foil on a 4 mm PVC substrate. Stencil openings varied between 400 µm, 500 µm and 600 µm. The highest shear values have been collected for the 600µm opening. Bigger openings are not used to avoid excessive squeeze-out of the glue while placing the sensors.

To evaluate the mechanical strength of the glued connection between the sensors and the Cu/Polyimide substrate, systematic quantitative analysis has been conducted with an in-house shear tester. A double-sided sheet with copper on one side and PI on the other side was glued onto 4 mm thick PVC substrates. Three samples were prepared for each side facing upwards, combining to six total samples.

A stencil was prepared to print a defined amount of silver glue on the specified piezo positions. Next, square piezoelectric elements (700 x 700 µm, height: 550 µm) were placed into the wet glue with a pick and placer machine. After curing at 120 °C for 20 min in the oven and cool down, the shear tests were conducted. Figure 20 shows images of the several process steps. Curing could to a bulging of the PVC substrate.

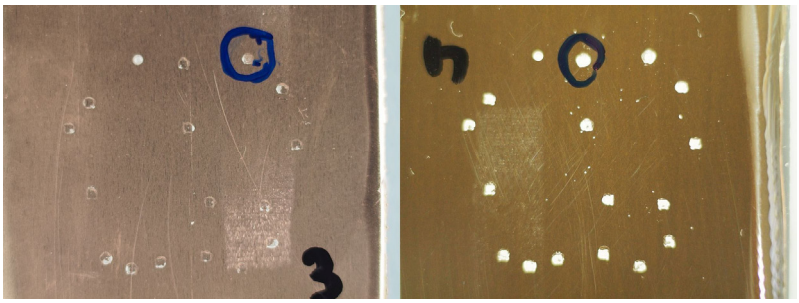

Figure 17: After shearing the piezos on Cu foil (lower left), shearing on the PI side (lower right), more glue is left on the PI surface.

Table 1 shows the mean shear force and the standard deviation for the Cu and the PI substrate. Out of 96 placed elements, four showed significantly lower shear values (<300 g) than the rest. Local impurities of the substrates are assumed to be the reason for this. They are excluded from the mean and standard deviation calculation. The measured shear values have to be scaled down to the final sensor surface area.

The values should guarantee firm mechanical connection that also withstands the forces exerted by the sawing blade.

Sample	Mean (g)	Std (g)	Mean (g)	Std (g)
1 – Cu	1288.6	388.9	1330.2	365.5
2 – Cu	1261.9	393.9		
3 – Cu	1442.7	271.9		
4 – PI	1482.2	213.0	1743.4	400.6
5 – PI	1933.4	446.5		
6 – PI	1802.0	351.9		

Table 1: Mean shear force and corresponding standard deviation of the shear tests performed on PC 3000 silver glue.

3.8 Matching options

3.8.1 TMM4

The acoustic impedance of Rogers TMM4 an aluminum oxide composite with of 6.4 MRayl acoustic impedance is near optimal for a single-layer matching between PZT and water. TMM4 is a very stiff, mechanical mil-and drillable material and exhibits low water absorption. Besides being a strong electrical insulator, thermal conductivity of TMM4 is quite high.

This is helpful for correct water temperature measurements, as the USCT temperature sensors are situated behind the TMM4 plate.

3.8.2 Silver glue and foil as matching

In collaboration with the TU Delft, an alternative design approach was followed with the idea to suppress lateral waves by replacing the stiff matching layer by a composite material of conductive silver glue with a thin sheet of metallic foil as common ground connection and matching layer.

Conductive silver glue, for instance Heraeus PC3000, is available with acoustic impedances suitable as a matching layer for PZT and water.

One approach is the application on the PZT base material, forming here the composite, which can be afterwards structured by sawing. Another approach is to glue a whole disc of the matching layer/PZT composite material onto the flex print. Alternatively, LASER cutting can structure transducers at arbitrary positions and in arbitrary shape. The constraint of the sensor positions to the octagon grid is obsolete. Additionally, LASER cutting results in conical cuts which should lead to varying aspect ratio which should lead to a frequency spreading and damping of unwanted spurious lateral oscillation modes.

Finally, a thin layer of foil is required for common ground connection. Usually, aluminum foil is used while tin was considered as potential option too having a fitting acoustic impedance and a lower better fitting sound speed.

Difficulties in this approach are a planar application of silver glue and a planar application of the ground foil (Figure 18). To provide additional support for the foil, an aluminum spacer ring (Figure 18) with the same thickness as the sensors was designed to be placed on the outside edge of the TAS. Waterproofing is achieved with a thin layer of parylene.

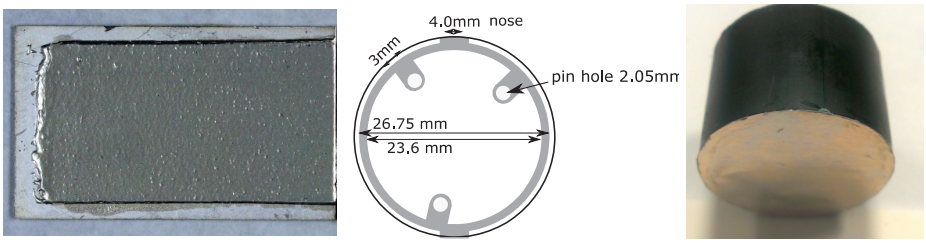

Figure 18: Left: Aluminium foil + PC 3000 silver conductive, middle: stainless steel spacer, right: transducer prototype with aluminum foil as common ground on the front side.

4 Evaluations and results

4.1 TMM4 matching layer

Figure 19 shows the assembled prototype with a TMM4 matching layer from front and rear. Due to process difficulties, 7 out of 17 sensors were working after final assembly. Figure 20 shows a frequency over angle plot from one of the elements and the corresponding pressure over frequency for the main direction perpendicular to the sensor surface. The electrical characterization of the same element can be observed in Figure 20 right.

Mean and standard deviation of important acoustic parameters are given in Table 2.

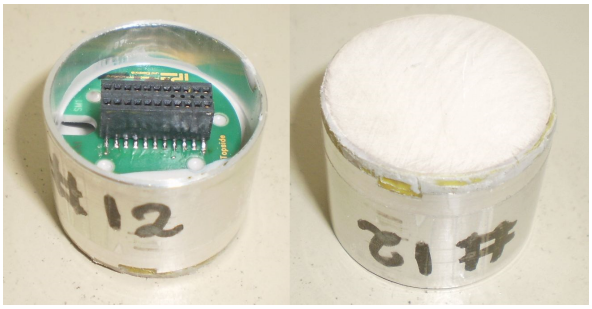

Figure 19: Assembled TAS 2.5 prototype. The rear side is filled with PU for mechanical stabilization (left). A TMM4 plate acts as a matching layer to water (right).

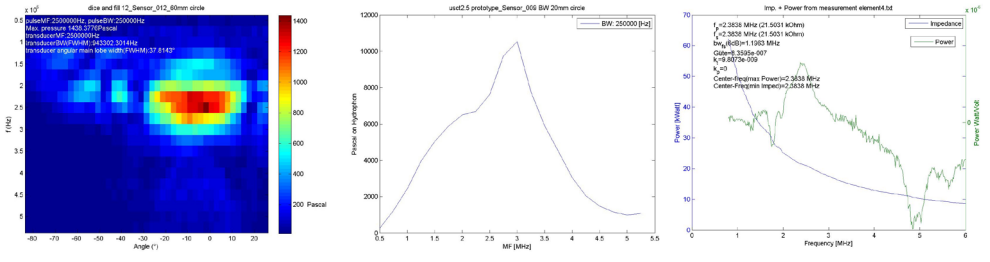

Figure 20: Frequency over angle for one element of transducer 1 (left). Pressure over frequency for main direction (middle). Corresponding electrical characterization from a –Impedance-Phase-analysator with only weakly pronounced serial and parallel resonances from the piezoelectrical material (right).

	BW (MHz)	Opening angle (°)	Pressure (Pa)
Mean	0.82	28.52	532.39
Std Dev	0.18	10.46	617.77

Table 2: Acoustic properties of prototype with TMM4 matching.

4.2 Tin foil matching layer

Figure 21 shows the final assembly steps for the prototype with a tin foil matching layer. Acoustic measurements are performed in the near future. The manufacturing process seems more challenging compared to a stiff matching layer and has to be optimized.

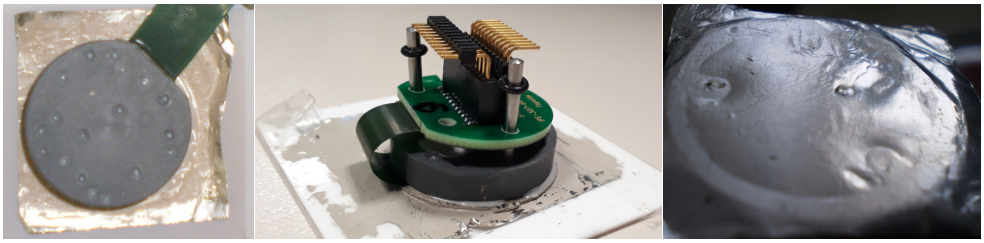

Figure 21: Left: Holes of the PVC substrate filled with PU-tungsten composite backing material. The backing is only applied behind the sensor elements. The backing and flex print are glued onto the tin foil matching. Middle: Pins align the back end of the PCB to fit in the casing later. Right: Tin foil matching layer after application.

4.3 Aluminium + PU matching layer

Figure 22 shows a frequency over angle plot from one of the elements expressing high BW and the corresponding pressure over frequency for the main direction perpendicular to the sensor surface. Figure 23 shows a frequency over angle plot from one of the elements expressing high OA and the corresponding pressure over angle at 2.4 MHz. Mean and standard deviation of important acoustic parameters are given in Table 3.

	BW (MHz)	Opening angle (°)	Pressure (Pa)
Mean	1.55	40.25	2969.86
Std Dev	0.57	21.78	3317.26

Table 3: Acoustic properties of prototype with PU + aluminum matching.

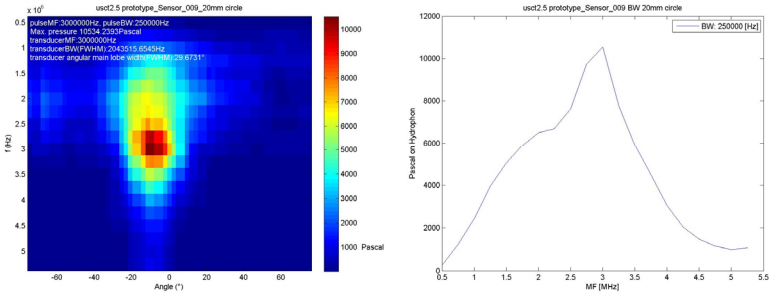

Figure 22: Frequency over angle shown for an element expressing high BW (left). pressure over frequency for emission in normal direction (right).

5 Discussion and conclusion

First prototypes were assembled with a flex print PCB in the described process and first results ares encouraging. The developed PU-tungsten composite backing material led to a significant increase in BW through improved acoustic matching to the rear of the transducer. While a in principle sufficient performance in soundpressure, bandwidth and open angle for the TMM4 + PZT piezo prototyped could be shown, the proution process is currently not finalized and as reliable a aimed for. The curently only semi-automatized process leads still to variations and in result to the failure of a signifcant portion of the transducer elements; especially in the glueing and filling step. This is currently under intensive investigation with further test prototypes. Further shear tests on the piezo have to be conducted to ensure all piezo elements reliable connected to the flex substrate to gain yield >95 % even after the sawing step. To prove the applicability and also potential mass producibility of the new design approach, complete TAS have to be built.

References

[1] [Online]. Available: http : / / www . wcrf . org / int / cancer - facts - figures / data - specific -cancers/breast-cancer-statistics..

[2] [Online]. Available: http://www.who.int/cancer/detection/breastcancer/en/index1.html..

[3] James S Michaelson et al., „“Predicting the survival of patients with breast carcinoma causing tumor size,“ Cancer, 2002.

[4] Ruiter et al., „Realization of an optimized 3D USCT,“ SPIE 7968, Medical Imaging 2011: Ultrasonic Imaging, Tomography, and Therapy,, 2011.

[5] T. H. M. Z. C. K. N. R. H. Gemmeke, „3D ultrasound computer tomography. hardware setup, reconstruction methods and first clinical results.“.Nuclear Instruments and Methods in Physics Research Section A: Accelerators, Spectrometers, Detectors and Associated Equipment.

[6] Gemmeke et al., „An improved 3D Ultrasound Computer Tomography system". IEEE International Ultrasonics Symposium., 2014.
[7] G. Göbel, „Entwicklung von Ultraschallsensorarrays mit miniaturisierten Komponenten," Diploma, KIT, 2002.
[8] M. Zapf, „Simulation eines Ultraschalltomographen im k-space," in Master thesis for Hochschule Karlsruhe (University of Applied Science), Karlsruhe, 2010.
[9] L. Petzold, „Aufbau eines Messplatzes zur Ermittlung der Schallfeldcharakteristik," Master thesis, KIT, 2006.
[10] G. Shah, „Auto-Calibration of Ultrasound Transducer Characterization Setup," Master thesis, KIT, 2015.
[11] P. Pfistner, „Composite-based ultrasound transducers for a 3D-Ultrasound computer tomograph," Master thesis, KIT, 2017.
[12] B. Kohout, „ Finite Elemente Simulation von Ultraschallwandlersystemen für die Ultraschall Computertomographie," KIT, Diploma , 2010.
[13] G. S. M.Zapf, „Aperture optimization for 3D ultrasound computer," IEEE UFFC Symp., 2007.
[14] N. R. H. Gemmeke, „3D ultrasound computer tomography for medical," Nuclear Instruments and Methods in Physics Research Section A: Accelerators, Spectrometers, Detectors and Associated Equipment, 2007.